THE UNCONTROLLED REENTRY OF PROGRESS-M 27M

Carmen Pardini[(1)], Luciano Anselmo[(2)]

[(1)] Space Flight Dynamics Laboratory, ISTI/CNR, Via G. Moruzzi 1, 56126 Pisa, Italy (Carmen.Pardini@isti.cnr.it)
[(2)] Space Flight Dynamics Laboratory, ISTI/CNR, Via G. Moruzzi 1, 56126 Pisa, Italy (Luciano.Anselmo@isti.cnr.it)

ABSTRACT

Uncontrolled reentries of sizable space objects are becoming of growing concern due to the increase of space activities around the Earth and population on the ground. After providing an updated review of various aspects of the problem, this paper presents the exemplar case of Progress-M 27M, whose control was lost immediately after launch, on April 28, 2015, and which reentered on May 8. As in similar previous occurrences, the Space Flight Dynamics Laboratory of ISTI/CNR, in Pisa, was in charge of reentry predictions for the Italian civil protection authorities and space agency. The first prediction was issued in the morning of April 30, in the morning of May 7 the only potentially risky reentry trajectory over central Italy was identified, and in the afternoon of May 7, about 12 hours before the actual reentry, any residual risk for Europe and Italy was finally excluded.

1. CATEGORIES OF UNCONTROLLED REENTRIES

The space objects subjected to uncontrolled reentries can be roughly grouped in five orbital categories:

1. Nearly circular low Earth orbits (LEO), with mean eccentricity $e \leq 0.015$, whose evolution is dominated by atmospheric drag;
2. Low or moderate mean eccentricity ($0.015 < e \leq 0.5$) orbits in LEO, or crossing both the LEO and the medium Earth orbits (MEO) regions, whose evolution is mainly driven by atmospheric drag around the perigee;
3. High mean eccentricity orbits ($e > 0.5$), whose evolution is driven by luni-solar third body attraction coupled with J_2, but for which the atmospheric drag at the perigee can play an important role at the end of the lifetime;
4. High mean eccentricity orbits ($e > 0.5$), whose evolution is dominated by luni-solar third body attraction coupled with J_2, with minor influences from solar radiation pressure;
5. Orbits initially above LEO, whose evolution is dominated by solar radiation pressure [1] [2].

The relatively massive intact objects for which reentry predictions are relevant are typically characterized by an area-to-mass ratio $A/M < 0.1$ m^2/kg, so the fifth category does not generally apply. Among the others, only for the objects belonging to the fourth category it is often possible to predict accurately in advance the location and time of atmospheric reentry. In fact, due to the Equivalence Principle and to the absolute predominance of gravitational forces, the orbit evolution does not (significantly) depend on the object physical characteristics and attitude, often unknown or known with considerable uncertainty, so it can be accurately modeled well in advance, if a reliable orbit determination is available. For example, the unidentified artificial object WT1190F, found in trans-lunar orbit and probably a remnant of the lunar exploration program, was predicted to impact a specific location of the Earth, 40 days before reentry, occurred on November 13, 2015, at 6:20 UTC, with a time error of less than one minute.

Unfortunately, this situation does not apply to the first three categories, where the complex interaction between the decaying space object and the Earth's thermosphere prevents the accurate prediction of a reentry location and time even a few hours before the event. For this reason, in most cases the reentry predictions of uncontrolled satellites are characterized by considerable uncertainties [3] [4] [5].

The large majority of the potentially risky uncontrolled objects belong to the first two categories. Concerning the first category, thermospheric drag is effective along the entire trajectory, whose semi-major axis progressively contracts, leading ultimately to reentry. Conventionally, the orbital motion ends when the object reaches the atmospheric interface at the altitude of 120 km, with a flight path angle slightly negative, but close to zero (tangential reentry). At this point, a final plunge in the densest layers of the atmosphere is unavoidable, even though, in certain cases, if some lift force builds up, a skip reentry may occur, with the object briefly bouncing back above 120 km, describing a ballistic arc, and falling again towards the Earth.

The orbits of the objects belonging to the second category are principally affected by thermospheric drag around the perigee, where most of the mechanical energy is dissipated. This mainly produces a progressive decrease of the apogee height, i.e. a progressive circularization of the orbit. When the orbit becomes nearly circular, what already said for the first category applies. However, it should be pointed out that a small

residual eccentricity, of the order of 0.001, cannot be eliminated in practice (this applies also to category one objects), and that in certain cases the reentry occurs when the circularization process is still underway and not yet completed, with $e > 0.015$.

The evolution of the apogee and perigee height of the objects belonging to the third category is driven by luni-solar perturbations, but the perigee altitude decrease is not always enough to cause a direct collision course with the Earth, as happens for category four objects. The evolution is therefore much more complicated and difficult to predict. The dive of the perigee in the thermosphere contributes, of course, to the orbit evolution, in terms of apogee and eccentricity decrease. In many cases a transition to the second category may occur. However, the perigee may also plunge several times well below the conventional atmospheric interface at 120 km, avoiding immediate reentry and regaining space each time to complete a further elliptical orbit. This situation is relatively common for satellites in Molniya orbits, which can experience aerodynamic fragmentations during these extremely low endo-atmospheric perigee passes. In these cases, the final decay of the main object occurs only when the combined effects of gravitational and air drag perturbations shift the perigee height below 50 km.

2. PHASES OF UNCONTROLLED REENTRIES

The objects belonging to the first two categories described in the previous section are subjected to a progressive mechanical energy loss due to thermospheric drag, with the consequent decrease of the semi-major axis. The atmospheric capture occurs when the objects, moving at that point in nearly circular orbit and with a slightly negative flight path angle, with a relative velocity of more than 7 km/s, descend at a height in between 120 and 110 km, initiating the reentry, i.e. the endo-atmospheric phase of their flight.

Even though some appendages and loose parts (like antennae, booms and solar panels) might already break away in such earlier phase, in general the main body of intact spacecraft and rocket stages fragments below the altitude of 80 km, due to a combination of thermal and aerodynamic loads. Therefore, the motion of a reentering object can be consistently modeled with the methods of orbital dynamics down to an altitude of 80-90 km. For this reason, very often reentry predictions epochs refer not to the crossing of the atmospheric interface, at 120 km, but to the altitude of 80 (or 90) km. For instance, current USSTRATCOM reentry assessments refer to 80 km and this is also roughly the altitude at which a reentry event becomes visible to eyewitnesses on the ground (if any). Last, but not less important, this is the lowest height for which a prediction is possible for any generic object, without a detailed knowledge of its design and construction details, coupled with a sophisticated endo-atmospheric fragmentation analysis.

Spacecraft or rocket bodies not specifically designed to survive the reentry, which is generally the norm in case of uncontrolled orbital decay, cannot avoid a catastrophic breakup below the altitude of 80 km. For intact objects with an initial dry mass of 800 kg or more, a mass fraction comprised between 60% and 95% is usually completely melted at high altitude [3] [4] [5]. The surviving fragments, accounting for the remaining 5% to 40% of the total mass, will instead reach the ground, distributing them in a “footprint” which can be as long as 2000 km, aligned with the sub-satellite trajectory [6]. The cross-track dispersion, due to the fragmentation processes, lift forces and winds (during the fall through the stratosphere and troposphere) is typically less than 50 km with respect to the sub-satellite ground track [6] [7]. It should also be emphasized that in the last 15 km the heaviest and fastest surviving debris falls nearly vertically, i.e. with a flight path angle close to –90° [4] [5].

The trajectories of the surviving fragments depend on their release time, melting history and physical characteristics. Those with a lower area-to-mass ratio tend to impact the ground earlier towards the tip of the footprint, while those with a higher area-to-mass ratio tend to fall later towards the heel [6]. Most of the macroscopic fragments impact the ground between 5 and 25 minutes after reentry at 80 km, but in certain cases debris may hit the Earth’s surface after 45 minutes [4] [8] [9].

Concerning the reentries belonging to the third category, aerodynamic fragmentations are possible, before atmospheric capture of the main object, at each perigee pass below 110–120 km. At the atmospheric interface (120 km) the relative velocity is around 10 km/s and the flight path angle may be lower than –5°. Moreover, the main object can survive several perigee passes at 80-90 km without further breakup. When the atmospheric capture occurs, the surviving debris is scattered over a significantly shorter footprint and the dispersion of the impact times is quite smaller. However, the details depend on the specific characteristics and final evolution of the parent object trajectory.

In the case of high eccentricity orbits dominated by luni-solar third body perturbations and intersecting the Earth’s surface (the fourth category of the previous section), the possible impact geometries may be extremely varied, as well as the relative velocities and flight path angles at the atmospheric interface. In general the reentries are faster and steeper, the surviving

mass lesser, due to considerably higher heat peak loads and cumulative absorption, and the ground dispersion of the fragments smaller, both in space and in time. As an example, for WT1190F the relative impact velocity, at the atmospheric interface, was around 11 km/s and the flight path angle was approximately −20°.

3. ORBIT DETERMINATION DATABASES

The most complete catalog of artificial objects in orbit around the Earth is maintained by the US Strategic Command (USSTRATCOM). Currently it includes more than 17,600 objects, of which more than 6200 are intact payloads and upper stages, mostly abandoned, while the rest is just debris. The catalog is officially available to registered users through the Space-Track Organization (www.space-track.org). However, orbits are available only for unclassified objects, making approximately 88% of the total. Sensitive military and intelligence spacecraft, together with the related upper stages, mission released objects and, often, debris, are listed, but their orbits are not provided. Moreover, in certain cases, it could take even three or four days (sometimes more) to include in the catalog reliable orbits and identifications of newly launched space objects. This means that for new space objects, with orbital lifetimes of less than a couple of days, reliable reentry predictions are often impossible.

Even with these important limitations, nothing else currently available may be compared to the USSTRATCOM catalog in terms of completeness, rate of updating and quality of the information provided. Orbits, when available, are supplied, for historical reasons, in the so-called Two-Line Elements (TLE) format [10] [11].

Over the years, a global network of very motivated and competent amateur astronomers, specialized in satellite observations, has proved itself very effective in identifying and tracking classified spacecraft with optical telescopes. The orbits obtained are generally quite accurate [12] and can be found in specialized websites, as Heavens-Above (www.heavens-above.com), developed and maintained by Chris Peat and hosted by DLR at the German Space Operation Centre (GSOC).

Additional tracking information obtained on request by European sensors can be very useful, as demonstrated by the reentry test campaigns promoted yearly by the Inter-Agency Space Debris Coordination Committee (IADC, www.iadc-online.org), but can only be supplementary and not substitutive of US space surveillance data. Only those collected by Russian sensors may offer, in certain reentry campaigns, as those promoted by the IADC, a practicable and effective alternative to USSTRATCOM orbits.

4. REENTRY PREDICTION UNCERTAINTY

Most of the uncontrolled reentries, including those with the highest casualty expectancy, are caused by thermospheric drag, so the accurate modeling of such perturbation is of paramount importance for reentry predictions as accurate as possible. To a large extent, a large fraction of the underlying uncertainties can be condensed into a single coefficient, the so-called ballistic parameter *B*, defined as follows:

$$B = \frac{C_D A}{M}, \tag{1}$$

where C_D is the drag coefficient, M the mass and A the average cross-section. In many cases the mass, the shape, the size and the attitude of the reentering object are not known, or approximately known, so the area-to-mass ratio may be affected by a significant uncertainty. The drag coefficient is uncertain as well, being a complex function of the atmosphere composition, density and temperature, and of the shape, size, surface composition and temperature of the object. Moreover, for a given atmospheric density, C_D also incorporates the errors of the model itself [13] [14] [15] [16] [17] [18].

Therefore, for the reentering objects belonging to the first two categories of Section 1, by far the most frequent, the prediction uncertainty is dominated by the modeling of thermospheric drag, which is characterized by inherent inaccuracies and biases related to the satellite physical properties and attitude, to the thermospheric density model itself, and to the prediction of solar and geomagnetic activity affecting the atmospheric temperature, and then the density, as a consequence. This means that even when the best practices are adopted and the best data available are used, the a priory uncertainty of the reentry predictions can be quite significant.

Focusing the attention on the last USSTRATCOM reentry predictions (www.space-track.org), they are currently based on orbits with a mean epoch of 5.0 ± 4.3 hours (1σ) before decay, with a cumulative non-Gaussian distribution detailed in Tab. 1. Comparing the last reentry predictions with actual observations in the 28 cases in which eyewitnesses on the ground were able to observe the reentry, from June 2010 to March 2016 [19], the results presented in Tab. 2 were found for the statistical distribution of the prediction uncertainty.

As an example, a reentry time uncertainty of ± 30%, able to include 90% of the events in the uncertainty window, applied to a trajectory propagation starting five hours before reentry, i.e. at the mean epoch of the last typically available orbit, corresponds to ± 1.5 hours, i.e.

to a couple of orbit tracks around the Earth. Consequently, for uncontrolled reentries driven by thermospheric drag, it is not possible to predict a reentry location, which remains quite undetermined until the end, but it is only possible to identify the areas of the planet where the reentry may no longer occur within a given confidence level [20].

Table 1. Epoch of last USSTRATCOM orbit determinations before reentry, from December 22, 2014, to January 30, 2016. The mean value was 5.0 ± 4.3 hours (1σ) before decay.

Cumulative probability	Reentry time since last orbit epoch (hours)
2.0%	< 1
19.6%	< 2
33.3%	< 3
50.0%	< 4
72.5%	< 5
90.2%	< 10
96.1%	< 15
98.0%	< 20

Table 2. Observed uncertainty of last reentry predictions at 80 km obtained by comparing USSTRATCOM data with eyewitnesses sightings (from June 19, 2010, to March 10, 2016).

Cumulative probability	Percentage reentry time absolute error (±) of last prediction at 80 km
25.0%	< 5%
57.1%	< 10%
64.3%	< 15%
71.4%	< 20%
89.3%	< 30%
92.9%	< 50%
96.4%	< 60%
100.0%	< 70%

5. UPDATED REENTRY STATISTICS

Since 1957, on average, reentered in the atmosphere 54 payloads, 64 upper stages and 289 debris per year, i.e. 2-3 intact objects per week, either controlled or uncontrolled. During the last decade, reentered on average 42 payloads, 40 rocket bodies and 361 debris per year, i.e. 1-2 intact objects per week [5]. Considering the uncontrolled reentries of intact objects occurred in 2015, 62% (64) were payloads and 38% (40) were upper stages, but 79% of the mass (i.e. 82 metric tons) was concentrated in the latter and the remaining 21% (i.e. 22 metric tons) in the former ones, consisting of small satellites with a mass lower than 50 kg in 83% of the cases.

Analyzing the uncontrolled reentries of intact objects occurred from 2004 to 2015 and for which a USSTRATCOM post-reentry time assessment with a claimed error of ± 1 minute was available (for 287 rocket bodies and 59 payloads/platforms), it was found a slight prevalence, 53.5% vs. 46.5%, of reentries occurring in the southern hemisphere. This bias was probably a real effect, reflecting the pattern of launches, mission orbits and residual lifetimes during the considered time interval. In fact, the probability that it was just the product of chance was 1.9%. The southern hemisphere bias was smaller for upper stages (51.6% vs. 48.4%), with a probability of chance occurrence of 4.1%, and higher for payloads (62.7% vs. 37.3%), with a probability of chance occurrence of 1.6%.

Analyzing 331 uncontrolled reentries occurred from September 1992 to December 1996, Nicholas Johnson had instead found a prevalence of decays in the northern hemisphere (56.5% vs. 43.5%), much more marked for the objects staying in orbit less than 1 month (62% vs. 38%) [21]. This supported the conclusion that the launch pattern, the mission profile and the residual lifetime of the objects placed in orbit was a driver of the varying north-south asymmetry.

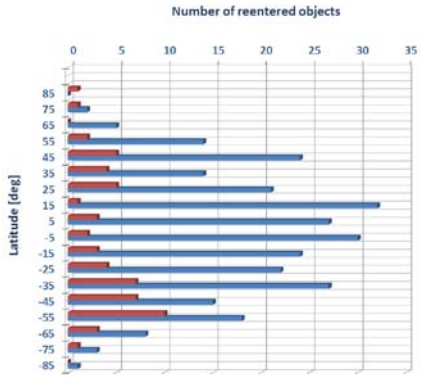

Figure 1. Distribution over 10° latitude bands of uncontrolled reentries occurred from 2004 to 2015 and for which a USSTRATCOM post-reentry time assessment with an error of ± 1 minute was available (payloads in red, rocket bodies in blue)

The reentry distribution over 10° latitude bands is presented in Fig. 1. 50.0% of the reentries occurred around the equator ± 30°, 42.5% at intermediate latitudes, between 30° and 60°, north and south, and 7.5% in the polar regions, above 60° of latitude north and south. The uncontrolled reentry flux for surface unit, compared with the average value over the total Earth surface, is detailed in Tab. 3.

Table 3. Uncontrolled reentry flux for surface unit, compared with the average value over the total Earth surface (2004-2015).

Latitude band	Reentry flux compared with the average
from 60° to 90°	38.8%
from 30° to 60°	99.5%
from 0° to 30°	102.9%
from –30° to 0°	98.3%
from –60° to –30°	132.7%
from –90° to –60	69.0%

It was lower than average, approximately one half, in the polar regions, relatively uniform and close to the average from 30° south to 60° north, and maximum, about 30% higher than average, from –60° to –30°. Considering all the uncontrolled reentries of intact objects occurred from 2004 to 2015 (722, of which 447 were rocket bodies and 275 payloads/platforms), the mean flux of decaying intact objects over the Earth was 1.05×10^{-7} km^{-2} per year. This implies, on average, an uncontrolled reentry over Italy every 28 years and over Europe every 10 months.

6. THE FAILURE OF PROGRESS-M 27M

Progress-M 27M (Fig. 2), launched from the Baikonur Cosmodrome aboard a Soyuz 2-1A rocket at 7:09 UTC on April 28, 2015, was the 150th Progress mission to fly since 1978 and the 2nd Progress craft to use the modern 2-1A version of the Soyuz launcher. After nearly nine minutes of powered flight, the cargo ship was separated in orbit, but it was quickly evident that communications with the ground were deteriorating.

Figure 2. A Progress-M cargo vessel, with a length of 7.23 m, a maximum diameter of 2.72 m and a maximum solar panels span of 10.6 m (courtesy of NASA)

The loss of telemetry from the Soyuz Block I third stage and the Progress spacecraft in the crucial seconds around the shutdown of the upper stage and the separation of the spacecraft was a first sign of malfunction, indicating that a significant event had taken place at, or around, separation. In an attempt to gain time, the mission profile was changed from the rapid 4-orbit rendezvous to a 34-orbit flight plan, with docking with the International Space Station expected two days after launch.

Progress-M 27M (2015-024A) was later tracked in an orbit with an apogee 40 km higher than planned, while the third stage ended up into a lower orbit with a 20 km deviation against the planned apogee. At least 44 pieces of debris were detected close to the spacecraft by the US Space Surveillance Network and later on the cargo ship was found to be in a rapid tumble around its long axis, with body rates in excess of 60° per second, confirming a loss of control. After repeated vain attempts to regain control of the vehicle, the mission was officially declared lost by the Russian Space Agency on April 29, 2015. That same day, at 7:32 UTC, the Soyuz third stage (2015-024B), with a mass of 2300 kg, reentered the atmosphere after 17 orbits.

With no ability to command Progress-M 27M for a safe return, the out of control supply vessel was irremediably doomed to an uncontrolled reentry. Starting from an orbit of around 189 × 269 km, inclined by nearly 52°, the reentry was expected within two weeks from the failure. Considering the launch mass of 7289 kg, a dry mass in excess of 5 metric tons and the presence on board of 1373 kg of highly toxic propellants (UDMH and N_2O_4), the uncontrolled reentry was expected to violate the worldwide alert casualty expectancy threshold of 1:10,000 [22] [23] [24] [25], even though a detailed fragmentation and demise analysis was not available.

A number of parts were presumed to survive reentry. The components with the highest probability of reaching the ground were the docking mechanism and the spherical pressurant tanks, compact in size and consisting of titanium alloy. An additional unknown were the tanks holding the very toxic UDMH and N_2O_4 propellants. However, due to the very short permanence in orbit of the vehicle, it was unlikely that the propellants had time to completely freeze. Consequently, their dispersion at high altitude during the reentry was considered the most probable scenario.

7. REENTRY PREDICTIONS

Taking into account the orbit inclination of Progress-M 27M, a reentering debris impact was a priori possible in the latitude belt between 53° south and north, therefore including Italy and a large fraction of Europe. Assuming a debris footprint of 800 km and the actual distribution of seas and land, the a priori probability of no impact on the ground was approximately 62%, reduced below 50% in case of a debris footprint 2000 km long [26] [27].

As in previous similar occurrences since 1979, the Space Flight Dynamics Laboratory of ISTI/CNR, in Pisa, was in charge of the reentry predictions for the Italian civil protection authorities and space agency. Fig. 3 shows the time evolution of the mean observed semi-major axis from the TLEs issued by USSTRATCOM. In the final decay phase, orbital data was only sparsely available, with the final data set epoch at 19:30 UTC, when Progress-M 27M was still more than six hours away from reentry. Also, the data sets issued in between the last propagated by ISTI/CNR, with epoch at 12:12 UTC, and the last available, with epoch at 19:30 UTC, showed irregular slowing or rushing in the spacecraft decay rate, leading to questions on the quality and reliability of the data.

The ballistic parameter estimates and the reentry predictions were carried out, respectively, with the CDFIT and SATRAP software tools [17] [28]. The thermospheric density model adopted thorough the campaign was NLRMSISE-00 [29], with the appropriate observed and predicted solar flux and geomagnetic activity indices. Concerning the estimation of the ballistic parameter *B*, the results are summarized in Fig. 4. After remaining substantially stable during the first 5 days of the campaign ($B \approx 5.3 \times 10^{-3}$ m^2/kg), from 2.91 to 0.82 days before reentry *B* increased steadily by nearly 27%, then decreasing by 10% during the last day. Such kind of variations is not unusual for uncontrolled objects in extremely low orbits. Moreover, the time interval of interest was characterized by a sharp increase of solar activity, with the flux at 10.7 cm passing from 100 standard flux units at the beginning to 155 standard flux units at the end, and by a small geomagnetic storm on May 6.

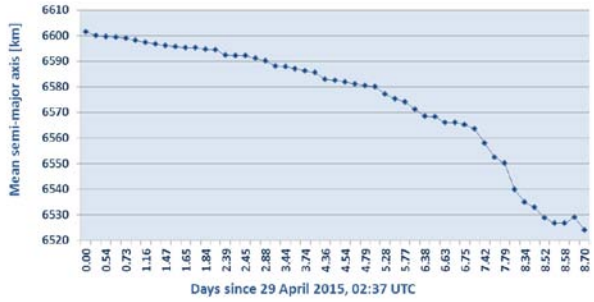

Figure 3. Time evolution of the mean observed semi-major axis of Progress-M 27M from the USSTRATCOM TLEs

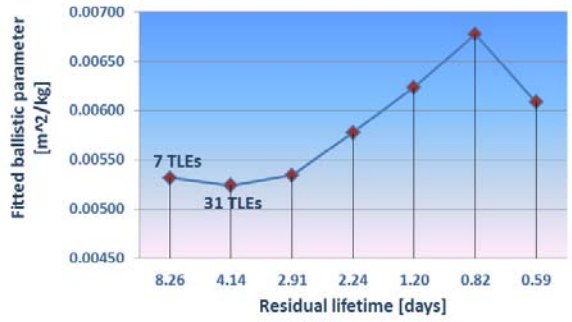

Figure 4. Evolution of the ballistic parameter of Progress-M 27M estimated during the reentry campaign

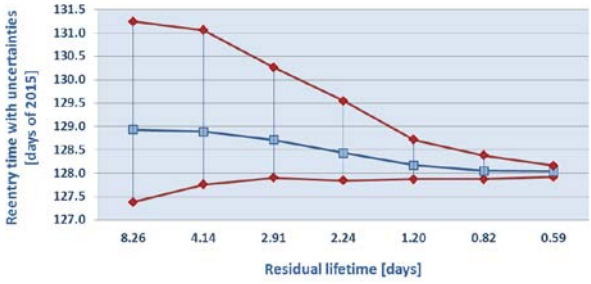

Figure 5. Evolution of Progress-M 27M reentry predictions and uncertainty windows (UTC)

In total, 7 reentry predictions at 80 km were issued to the Italian authorities (Fig. 5 and Tab. 4). The first uncertainty window was computed by varying by ± 20% the estimated ballistic parameter, while the following five windows were obtained with a ballistic parameter variation of ± 30%. For the last one, the start of the window was computed by increasing by 30% the last *B* estimated, while the end of the window was obtained by increasing by 30% the final nominal residual lifetime.

Table 4. Progress-M 27M reentry predictions and uncertainty windows issued by ISTI/CNR (UTC).

Propagation start epoch	Start of reentry uncertainty window	Nominal reentry prediction at 80 km	End of reentry uncertainty window
20150429 20:00	20150507 09:07	20150508 22:18	20150511 05:51
20150503 23:01	20150507 18:10	20150508 21:16	20150511 01:16
20150505 04:49	20150507 21:39	20150508 17:11	20150510 06:21
20150505 20:39	20150507 20:12	20150508 10:22	20150509 13:04
20150506 21:35	20150507 20:59	20150508 04:02	20150508 17:10
20150507 06:39	20150507 20:58	20150508 01:12	20150508 09:06
20150507 12:12	20150507 22:05	20150508 00:58	20150508 03:48

8. REENTRY GROUND TRACKS

With an orbit determination corresponding to an epoch 1.2 days before reentry, the reentry ground track still included in the uncertainty window is shown in Fig. 6. For the way in which the figure was obtained, not for inherent computational inaccuracies, the plotted sub-reentry ground track was reasonably accurate around the "nominal" reentry epoch, but, due to the size of the

uncertainty window, was affected by a westward cross-track error of 210 km at the window start and by an eastward cross-track error of 300 km at the window end.

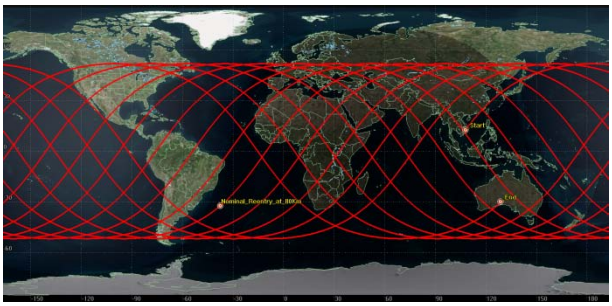

Figure 6. Progress-M 27M sub-reentry (at 80 km) ground track included in the uncertainty window corresponding to the 5th ISTI/CNR reentry prediction

The following prediction, the 6th issued by ISTI/CNR, was based on an orbit determination corresponding to an epoch 0.82 days before reentry. The reentry ground track still included in the uncertainty window was considerably reduced, as shown in Fig. 7, and comprised only one potential reentry opportunity at 80 km over Italy, around 5:53 UTC of May 8. Concerning Europe, the reentry opportunities still included in the uncertainty window are detailed in Fig. 8.

Finally, at 14:00 UTC of May 7, i.e. 12 hours and 20 minutes before the actual reentry, ISTI/CNR issued the 7th reentry prediction, based on an orbit with an epoch corresponding to 12:12 UTC. The new, reduced, uncertainty window finally allowed the exclusion of Europe from the reentry risk, as shown in Fig. 9, but no further prediction was issued later on because the new orbit determination data available until reentry was not considered reliable enough.

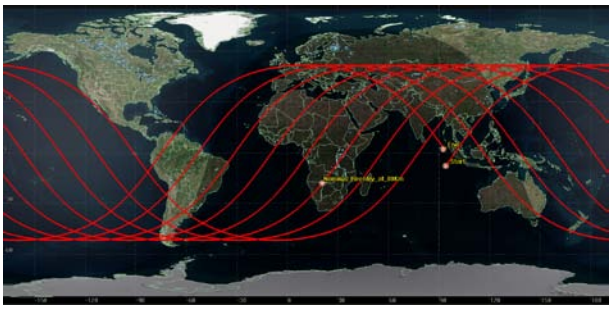

Figure 7. Progress-M 27M sub-reentry (at 80 km) ground track included in the uncertainty window corresponding to the 6th ISTI/CNR reentry prediction

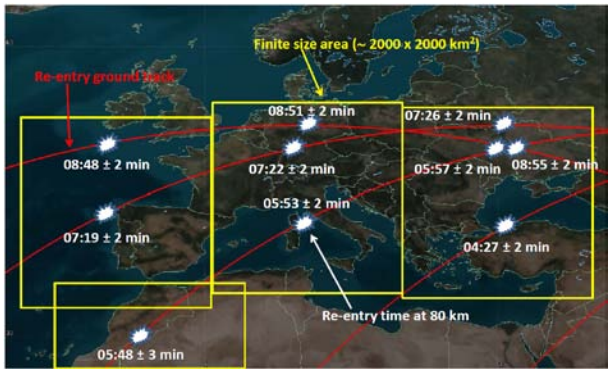

Figure 8. Progress-M 27M sub-reentry (at 80 km) ground track over Europe, and corresponding reentry times in each geographic area, included in the uncertainty window of the 6th ISTI/CNR reentry prediction

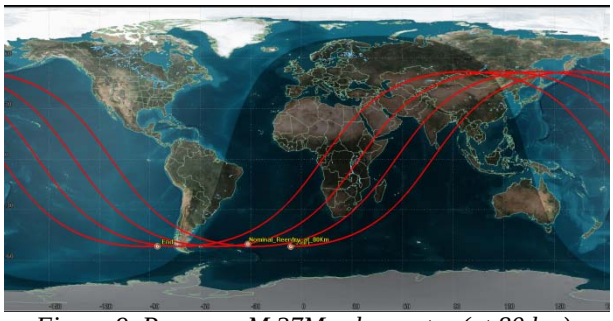

Figure 9. Progress-M 27M sub-reentry (at 80 km) ground track included in the uncertainty window corresponding to the 7th ISTI/CNR reentry prediction

The reentry at 80 km of Progress-M 27M at last occurred on May 8, 2015, at 2:20 UTC ± 1 minute, over the Southern Pacific Ocean, based on the post-reentry assessment carried out by the Joint Space Operations Center (JSpOC) of USSTRATCOM with classified satellite infrared observations (Fig. 10). This estimate placed the orbital decay of the unlucky cargo ship anywhere from 1300 to 350 km off the southern Chilean coast. Nevertheless, no sighting was reported and no debris was recovered.

Figure 10. Progress-M 27M JSpOC reentry assessment at 80 km with ± 1 minute uncertainty

9. REENTRY PREDICTIONS ACCURACY

The Progress-M 27M reentry predictions campaign was set up in a few hours for an object having less than 10 days of residual lifetime. Moreover, the rotational dynamics was completely unusual, quite complex and rapidly evolving, and both solar and geomagnetic activity were on the rise. However, the results obtained where consistent and satisfactory, allowing the timely issuing of useful data and products for civil protection applications [20].

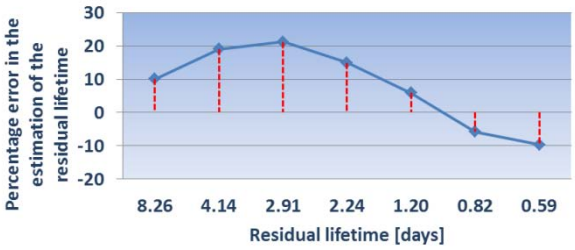

Figure 11. Percentage error of each reentry prediction issued by ISTI/CNR

The errors affecting the reentry predictions issued by ISTI/CNR are summarized in Figs. 11 and 12. The worse prediction was the third one, around three days before reentry, characterized by an over-estimation of the residual lifetime of little more than 20%. This was probably due to the occurrence, the following day, of a small geomagnetic storm, whose main effect was an increase of thermospheric density and a consequent acceleration of the decay. Nevertheless, a progressive acceleration of the Progress-M 27M decay was a constant of the campaign (see Fig. 5), due to a significant growth of solar activity and extreme ultraviolet emissions, leading to higher thermospheric density as well.

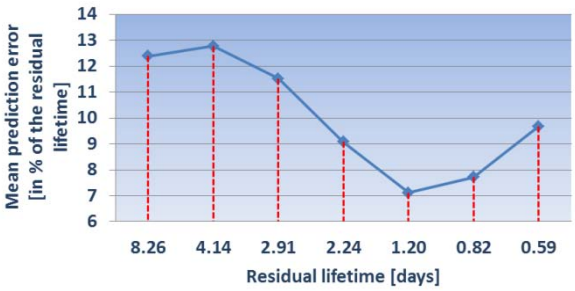

Figure 12. Running mean error of the reentry predictions issued by ISTI/CNR

The mean error of the predictions was approximately 12%, the residual lifetime was over-estimated in the first five and under-estimated in the last two, the most accurate estimates (with an error around 5%) were obtained around one day before reentry and the last prediction was affected by an error of approximately 10%. Therefore, the uncertainty windows adopted resulted fully appropriate, consistent and conservative through all the campaign.

The only significant problem encountered was the lack of reliable and consistent orbit determination data during the last 12 hours. Fortunately, a reentry over Europe and Italy had already been excluded at that time, but it was impossible to further reduce the uncertainty window on Africa, Asia and South America before the actual plunge of the spacecraft in the atmosphere.

10. ACKNOWLEDGMENTS

Part of the work described in this paper was carried out in the framework of the ASI-INAF agreement on "Detriti Spaziali: supporto alle attività IADC e validazione pre-operativa per SST" (F82I15000440005). We would like also to thank the USSTRATCOM and the Space-Track Organization for making available the two-line elements of Progress-M 27M and the data concerning historical reentries, the Space Debris Office of the European Space Agency for providing a couple of TLEs determined with the German TIRA radar and sharing relevant information, and the Mission Control Center of the Russian Space Agency for information exchange. Finally, some of the figures were generated with the AGI's Satellite Tool Kit (STK), Version 10.1.3.

11. REFERENCES

1. Pardini, C. & Anselmo, L. (2008). Long-Term Evolution of Geosynchronous Orbital Debris with High Area-to-Mass Ratios. Transactions of The Japan Society for Aeronautical and Space Sciences 51(171), 22–27.

2. Anselmo, L. & Pardini, C. (2009). Dynamical Evolution of High Area-to-Mass Ratio Debris Released into GPS Orbits. Advances in Space Research 43(10), 1491–1508.

3. Klinkrad, H., Fritsche, B., Lips, T. & Koppenwallner, G. (2006). Re-Entry Prediction and On-Ground Risk Estimation. In Space Debris – Models and Risk Analysis (Klinkrad, H., Ed.), Chapter 9, Springer Praxis Publishing Ltd., Chichester, UK, pp. 241–288.

4. Anselmo, L. & Pardini, C. (2005). Computational Methods for Reentry Trajectories and Risk Assessment. Advances in Space Research 35(7), 1343–1352.

5. Pardini, C. & Anselmo, L. (2013). Re-entry Predictions for Uncontrolled Satellites: Results and Challenges. In Proc. 6th IAASS Conference 'Safety is Not an Option' (Ouwehand, L., Ed.), ESA SP-715 (CD-ROM), European Space Agency, Noordwijk, The Netherlands.

6. Wilde, P.D. & Ailor, W. (Eds.) (2013). Re-Entry Operations Safety. In Safety Design for Space Operations (Sgobba, T., Allahdadi, F.A., Rongier, I. & Wilde, P.D., Eds.), Chapter 9, Elsevier & Butterworth-Heinemann, Oxford, UK, pp. 603–775.
7. Molczan, T. (2015). Re-Entry Sightings and Debris Recovery of 2008-010B Spain – 2015 November 03 UTC. Journal of Space Safety Engineering 2(2), 83–90.
8. Anselmo, L. & Pardini, C. (2013). Satellite Reentry Predictions for the Italian Civil Protection Authorities. Acta Astronautica 87(1), 163–181.
9. Pardini, C. & Anselmo, L. (2015). GOCE Reentry Predictions for the Italian Civil Protection Authorities. In Proceedings of 5th International GOCE User Workshop (Ouwehand, L. Ed.), ESA SP-728, European Space Agency, Noordwijk, The Netherlands.
10. Hoots, F.R. & Roehrich, R.L. (1980). Models for Propagation of NORAD Elements Sets. Spacetrack Report No. 3, Project Spacetrack, Aerospace Defense Command, United States Air Force, Colorado Springs, Colorado, USA.
11. Vallado, D.A., Crawford, P., Hujsak, R. & Kelso, T.S. (2006). Revisiting Spacetrack Report #3. Paper AIAA 2006-6753. Presented at the AIAA/AAS Astrodynamics Specialist Conference, Keystone, Colorado, USA.
12. Pardini, C. & Anselmo, L. (2009). USA-193 Decay Predictions with Public Domain Trajectory Data and Assessment of the Post-Intercept Orbital Debris Cloud. Acta Astronautica 64(7-8), 787–795.
13. Pardini, C. & Anselmo, L. (2001). Comparison and Accuracy Assessment of Semi-Empirical Atmosphere Models Through the Orbital Decay of Spherical Satellites. The Journal of the Astronautical Sciences 49(2), 255–268.
14. Pardini, C. & Anselmo, L. (2004). On the Accuracy of Satellite Reentry Predictions. Advances in Space Research 34(5), 1038–1043.
15. Pardini, C., Tobiska, W.K. & Anselmo, L. (2006). Analysis of the Orbital Decay of Spherical Satellites Using Different Solar Flux Proxies and Atmospheric Density Models. Advances in Space Research 37(2), 392–400.
16. Pardini, C. & Anselmo, L. (2008). Impact of the Time Span Selected to Calibrate the Ballistic Parameter on Spacecraft Re-entry Predictions. Advances in Space Research 41(7), 1100–1114.
17. Pardini, C., Anselmo, L., Moe, K. & Moe, M.M. (2010). Drag and Energy Accomodation Coefficients During Sunspot Maximum. Advances in Space Research 45(5), 638–650.
18. Pardini, C., Moe, K. & Anselmo, L. (2012). Thermospheric Density Model Biases at the 23rd Sunspot Maximum. Planetary and Space Science 67, 130–146.
19. The Aerospace Corporation (2016). Reentry Predictions. Center for Orbital and Reentry Debris Studies webpage (www.aerospace.org/cords/reentry-predictions/).
20. Pardini, C. & Anselmo, L. (2015). Satellite Re-entry Prediction Products for Civil Protection Applications. In Proc. 7th IAASS Conference 'Space Safety is No Accident' (Sgobba, T. & Rongier, I., Eds.), Springer International Publishing, Switzerland, pp. 453–462.
21. Johnson, N. (1997). The Re-Entry of Large Orbital Debris. In Space Safety and Rescue 1997 (Heath, G.W, Ed.), Vol. 96, Science and Technology series, Univelt Inc., San Diego, California, USA, pp. 285–293.
22. European Space Debris Safety and Mitigation Standard Working Group (2004). European Code of Conduct for Space Debris Mitigation, Issue 1.0, EDMSWG, 2004, p. 7.
23. JAXA (2011). JAXA Management Requirements 003 (JMR-003), Version B, Japan Aerospace Exploration Agency.
24. NASA (2012). Process for Limiting Orbital Debris, NASA-STD-8719.14, Revision A with Change 1, NASA Technical Standard, National Aeronautics and Space Administration, Washington, DC, USA, p. 44.
25. ESA Space Debris Mitigation Working Group (2015). ESA Space Debris Mitigation Compliance Verification Guidelines, Issue 1, European Space Agency, p. 28.
26. Matney, M. (2012). On the Probability of Random Debris Reentry Occurring on Land and Water. In Orbital Debris Quarterly News, Vol. 16, Issue 1, NASA Orbital Debris Program Office, p. 5.
27. Matney, M. (2012). On the Probability of Random Debris Reentry Occurring on Land and Water, Part II. In Orbital Debris Quarterly News, Vol. 16, Issue 2, NASA Orbital Debris Program Office, p. 6.
28. Pardini, C. & Anselmo, L. (1994). SATRAP: Satellite Re-entry Analysis Program. Internal Report C94-17, CNUCE Institute, CNR, Pisa, Italy.
29. Picone, J.M., Hedin, A.E., Drob, D.P. & Lean, J. (2002). NRLMSISE-00 Empirical Model: Comparisons to Data and Standard Models. In

Astrodynamics 2001, Advances in the Astronautical Sciences Series, Vol. 109, Univelt Inc., San Diego, California, USA, pp. 1385–1398.